Study of vortex dynamics in single crystalline $Ba_{0.54}K_{0.46}Fe_2As_2$ superconductor using dc and ac magnetization

D. Paladhi [a], C. Zhang [b, c], Guotai Tan [d], P. Dai [b], T.K. Nath [a, *]

[a] Department of Physics, Indian Institute of Technology Kharagpur, West Bengal, 721302, India
[b] Rice University, Physics and Astronomy Department, 6100 Main St, MS-61, Houston, TX, 77005, USA
[c] Wuhan National High Magnetic Field Center, School of Physics, Huazhong University of Science and Technology, Wuhan, 430074, China
[d] Beijing Normal University, Beijing, 100875, China

ARTICLE INFO

ABSTRACT

Due to relatively lower superconducting transition temperature(T_c), weaker anisotropy and larger coherence length, the overall strength of thermal fluctuations in iron-based superconductors seem to be intermediate between cuprates and more classical superconductors like Nb_3Sn. A detailed linear and non-linear ac magnetic susceptibility technique has been used as a probe to investigate the vortex-glass melting transition and vortex dynamics in an optimally doped p-type $Ba_{0.54}K_{0.46}Fe_2As_2$ good quality single crystal (RRR ≈ 10) under various fields and frequency range. Besides these, we have also constructed a vortex phase diagram in this compound using dc magnetization. Magnetic irreversibility temperature (T_{irr}) is the only temperature where solid vortex phase shows true zero resistance and has a great importance for technical applications of a superconductor. We have clearly observed that T_{irr} strongly depends on frequency and this dependency can be explained in the framework of vortex-glass phase transition model. From our experimental observations, we conclude that vortex-glass melting transition is second order in nature and vortex phase shows glassy character in this compound.

© 2016 Elsevier B.V. All rights reserved.

1. Introduction

It has been recognized that critical thermal fluctuation and disorder control the overall vortex dynamics in the mixed state of type-II superconductors. In the phase diagram of type-II superconductor there exists a new thermodynamic state called vortex glass phase which is actually a true superconducting phase with zero dc resistance [1]. Vortex glass phase is characterized by a nonzero Edwards-Anderson order parameter but does not have conventional off diagonal long-range order (ODLRO) [2]. The discovery of high-T_c type-II superconductivity in Fe-based materials [3–6] has ignited huge interest in the physics of vortex dynamics since these materials are thought to make a bridge between high-T_c cuprates and low-T_c BCS type superconductors. In the cuprate high temperature superconductors, critical thermal fluctuations of the 3D-XY universality class, due to the short superconducting coherence length and high transition temperature, determine the superconducting properties around T_c [7–12]. As a result solid

vortex phase melts into a liquid vortex phase below the superconducting transition temperature [13]. In iron-based superconductors, thermal fluctuations have also been observed but they are stronger in the 1111 compounds than in the 122 compounds [14,15]. The vortex melting transition can be either of a first order if solid phase is crystalline or second order if solid phase is glassy depending on the nature of pinning [13]. In iron arsenide $Ba_{0.5}K_{0.5}Fe_2As_2$ superconductor, second-order-type thermodynamic vortex melting transition has been observed experimentally and it may cross to a weakly first-order transition in high fields as confirmed from specific heat, thermal expansion and dc magnetization measurements [16]. Despite these, the evolution of vortex melting transition under different magnetic field and frequency regime needs further investigation, including nature of vortex melting transition and vortex phase in optimally doped (Ba, K) Fe_2As_2 single crystal. We have chosen ac susceptibility (ACS) technique to investigate the vortex dynamics where we actually measure the response of vortex lines to ac fields. Ac technique can yield extra information than dc resistivity since frequency can be varied in addition to temperature, dc field and ac field amplitude. The order of the vortex melting transition can be made possible to observe through ac susceptibility (ACS) by observing frequency

dependence of the magnetic irreversible temperature (T_{irr}). T_{irr} is a significant transition temperature from a state of flux pinning to a state of dissipative flux motion without pinning. T_{irr} changes with application of magnetic field and it provides a distinct phase boundary in the magnetic phase diagram of the vortex state called irreversibility line $H_m(T)$ or $H_{irr}(T)$. Irreversibility temperature (T_{irr}) can be determined from the third harmonic ac susceptibility measurement since it gives only nonlinear dissipation. In Y−Ba−Cu−O crystals, T_{irr} is independent of frequency suggesting a 1st order phase transition, while in Bi−Sr−Ca−Cu−O and Tl−⊕ Ba−Ca−Cu−O crystals T_{irr} strongly depends on frequency implying a 2nd order phase transition [17]. These findings have made newly discovered Fe-based superconductors more interesting to determine whether T_{irr} strongly depends on frequency or not in optimally doped $Ba_{1-x}K_xFe_2As_2$ single crystals. We have carried out detailed experimental investigation through linear and non-linear ac susceptibility measurements to study flux dynamics and frequency dependence of T_{irr} on single crystal $Ba_{0.54}K_{0.46}Fe_2As_2$ (BaK122). In this paper, our main focus is to show the frequency dependence of T_{irr} of BaK122 single crystal and to conclude the nature of vortex-glass melting transition. We have also done some investigations of vortex phase of BaK122 single crystal using dc magnetization and construct a vortex phase diagram. In this paper, we report detailed magnetization (ac and dc both) on BaK122 single crystal with $T_c = 38.5$ K. The results include: (i) clear observation of second magnetization peak (SMP) in magnetization hysteresis loops (MHLs), (ii) estimation of critical current density from MHLs using Bean's critical state model [18] with the correction [19] and their variation with magnetic field, (iii) obtaining the vortex phase diagram from magnetization data, (iv) temperature variation of fundamental and harmonic ac susceptibilities measured for several ac field frequency (f), dc field (H_{dc}) and ac field amplitude (H_{ac}) of BaK122 single crystal, (v) finally based on the above results understanding of the nature of vortex-glass melting transition and comparing of the results with cuprates and other iron based superconductors.

2. Experimental details and main results

The $Ba_{0.54}K_{0.46}Fe_2As_2$ single crystals were prepared by self-flux method [20]. The sample, with sizes of $\approx 2.5 \times 2.4 \times 0.4$ mm^3, is characterized by a $T_c = 38.5$ K and $\Delta T_c = 1.0$ K (offset-onset criterion). The crystals have been characterized by x-ray diffraction (XRD) at room temperature to confirm the absence of any foreign impurity phase. We have also carried out energy dispersive x-ray (EDX) analysis to know the exact chemical compositions of the crystals. For other measurements such as magnetization (ac and dc both) we have actually used a small single piece of sample that has been cleaved from the thick sample. The composition difference was negligibly small. Each of the layers can be easily cleaved from the rest. The temperature dependent magnetization data have been recorded in the zero-field-cooled (ZFC) mode during warming cycle using a superconducting quantum interference device-vibrating-sample-magnetometer (SQUID-VSM) (Quantum Design, USA) with magnetic fields up to 6 T for both out-of-plane ($H||c$) and in-plane (H⊥c) orientations. We have also measured magnetic hysteresis loops (MHLs) using the same instrument (SQUID-VSM) mentioned above for both out-of-plane ($H||c$) and in-plane (H⊥c) orientations. The temperature dependence of the higher harmonics as well as fundamental harmonics of ac-susceptibility has been measured at different ac and dc field amplitudes and frequencies. The ACS data have been recorded when the temperature is increased with a rate of 0.3 K/min.

Fig. 1(a) shows the recorded X-ray diffraction pattern at room temperature using a diffractometer (Panalytical X'Pert Pro) with Cu

K_α radiation ($\lambda = 1.542$ Å) and the observed pattern is very similar to the previously reported results [21]. For these measurements, a plate-like single crystal with dimensions of $2.5 \times 2.4 \times 0.4$ mm^3 was attached to a flat sample holder. The observation of only 00*l* Miller indices confirms that c-axis is perpendicular to the flat surface. Based on the $ThCr_2Si_2$ type structure, we have indexed all the observed reflection peaks which confirm phase purity of our $Ba_{1-x}K_xFe_2As_2$ single crystals. The FWHM of the 002 diffraction peak is only about 0.093° and it clearly indicates good crystalline quality of our sample. We have also carried out elemental analysis at eight different layers of the sample using energy dispersive x-ray analysis (EDX) in the electron probe micro analyzer of JEOL JXA-8200 superprobe. Treating the sample as $Ba_{1-x}K_xFe_2As_2$, the final potassium (K) content (x) was estimated by averaging over different points and it comes out to 0.46(1) which is close to the optimally doped composition. The single crystal of hole-doped $Ba_{0.54}K_{0.46}Fe_2As_2$ (BaK122) exhibited superconducting transition temperature at 38.5 K using magnetic measurement (shown in the inset of Fig. 1(b)) and this T_c value corresponds to the optimal doping in the phase diagram of $Ba_{1-x}K_xFe_2As_2$ [22]. We have carried out detailed dc magnetization study to construct the vortex phase diagram. Fig. 2(a) and (b) show isothermal magnetization curves M(H) up to ±60 kOe applied magnetic fields at various temperatures below T_c for $H||c$ and H⊥c orientations, respectively. From these data we have calculated critical current density in two different orientations using Bean's model [18] and extended Bean's model [19] and it is explained below. Finally we have presented fundamental as well as higher harmonic ac susceptibility data to investigate in details about its flux dynamics.

3. Analysis and discussion

3.1. Construction of vortex phase diagram using dc magnetization

Now in this section we have constructed the vortex phase diagram using dc magnetization measurements. From the magnetization vs magnetic field curves (MHLs), we observe a central peak at zero magnetic field and then magnetization decreases continuously with increasing magnetic field for H⊥c orientation. But for $H||c$ orientation it behaves differently: after the central peak observed at zero magnetic field, there is another peak at non-zero magnetic field and it is clearly visible from the peak (Fig. 3(b)) in current density calculated from MHLs when temperature is very close to T_c. This is called fishtail effect or second peak effect or peak effect (PE). This feature has also been observed in the clean high quality single crystal such as cuprate superconductors, Nb_3Sn [23], MgB_2 [24] and it may be induced by a different mechanism. In conventional superconductors like niobium, the occurrence of PE is observed just below H_{c2} and the two dimensional melting field H_m^{2D}, respectively. It has been attributed to the softening of the shear modulus [23]. In some cases such as bulk $REBa_2Cu_3O_{7-\delta}$ (REBCO), the anomalous second peak appears at different fields at different temperatures and in other cases such as Bi-based and Tl-based cuprates the peak position is temperature independent [25]. The origin of PE in REBCO and Bi- or Tl-based cuprates is different but have not got general consensus. In iron based superconductors small size normal cores may be the possible reason for PE [26]. Recently, Zhou et al. have investigated that PE in BaK122 type iron-based superconductors are accompanied with collective (or elastic) to plastic vortex pinning regime crossover (E-P crossover) [27] and small size normal cores are helpful for occurrence of E-P crossover [27]. At low temperature, we have not seen any second peak anomaly even for $H||c$ orientation because of shifting the peak position at high magnetic field beyond 60 kOe as shown in Fig. 2(a). The peak position (H_{SP}) gradually shifts to the low field region with increasing
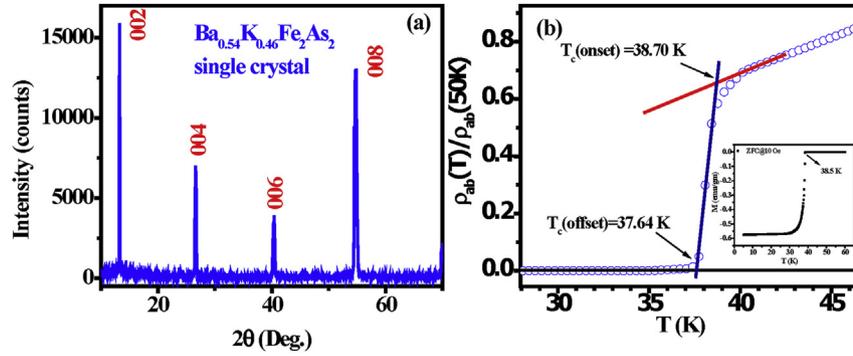
Fig. 1. (a) The high resolution x-ray diffraction pattern of $Ba_{0.54}K_{0.46}Fe_2As_2$ single crystal. (b) Temperature dependent in-plane resistivity of $Ba_{0.54}K_{0.46}Fe_2As_2$ single crystal in the vicinity of superconducting transition; inset shows temperature dependent magnetization data in the zero-field-cooled (ZFC) mode during warming cycle using a superconducting quantum interference device-vibrating-sample-magnetometer (SQUID-VSM) (Quantum Design, USA).
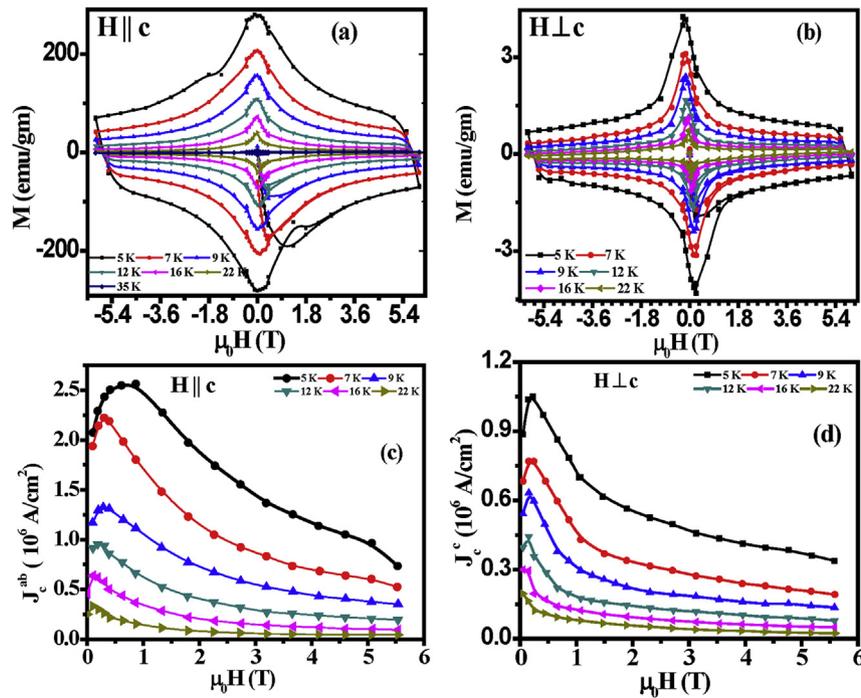
Fig. 2. Isothermal magnetization curves M(H) at different temperatures (a) for $H\|c$ direction and (b) for H⊥c direction. (c)–(d) Field dependence of the calculated critical current density from the Bean's critical state model corresponding to the above curves.

temperature which is clearly visible from Fig. 3(b). An estimation of the field dependent critical current density (J_c^{ab}) from isothermal magnetization hysteresis loops has been carried out with the framework of Bean's model [18] when magnetic field is applied parallel to the c-axis $H\|c$. When magnetic field is applied perpendicular to c-axis (H⊥c), the situation becomes complicated. Depending on the motion of Abrikosov vortices under Lorentz force, two different current densities exist in H⊥c orientation: one for the vortex motion parallel to the planes ($J_c^{\|}$) and another for the vortex motion across the planes (J_c^c). The formula derived by Gyorgy et al. [19] is mainly important for relatively large anisotropic materials. In our case anisotropy is low (~1–2). According to the Bean's model critical current density (J_c^{ab}) is given by $J_c^{ab} = 20\Delta M/[w(1 - w/3l)]$, where ΔM is measured in emu/cm^3, and the length l and the width w of the sample ($w < l$) are measured in cm. For H⊥c orientation we have used simplified method by assuming $J_c^{ab} = J_c^{\|}$ for calculating J_c^c which is described in Ref. [28]

and [29]. Fig. 2(c) and (d) show the field dependence of J_c^{ab} and J_c^c for $H\|c$ and H⊥c orientations where current densities decrease monotonously with magnetic field after a sharp peak at near zero field. The estimated J_c^{ab} and J_c^c at 5 K and 0 T are 2.0×10^6 A/cm^2 for $H\|c$ orientation and 0.9×10^6 A/cm^2 for H⊥c orientation, indicating good current carrying ability for promising technological applications. Fig. 3(b) shows that J_c^{ab} increases with the magnetic field after the first peak when applied magnetic is along the c direction. This is obviously due to second peak anomaly in MHLs. Peak in the $J_c^{ab}(H)$ (inset of Fig. 3(b)) separates a region of elastic vortex flow below the peak from plastic vortex flow above the peak, which may be related to the vortex glass melting transition. Corresponding to this $J_c^{ab}(H)$ curves we have defined three characteristic fields termed as peak field (H_{sp}), valley field (H_{min}), and irreversible field (H_{irr}). H_{irr} is defined as the points where J_c goes to zero which is shown in the inset of Fig. 3(b). The magnetic upper critical field (H_{c2}^m) has been estimated using the magnetization vs temperature curves (M-T)
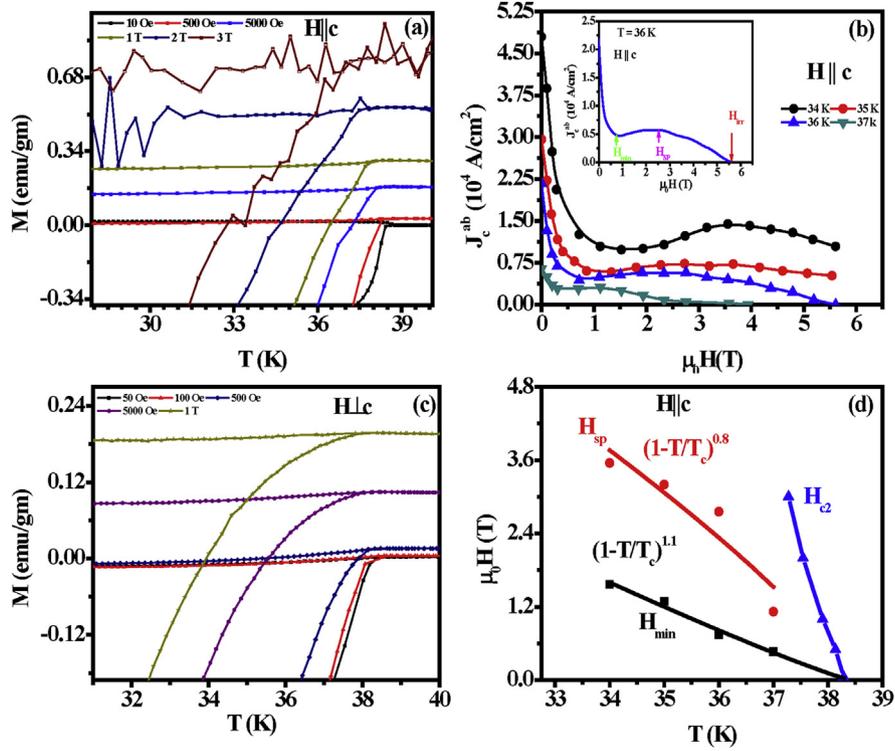
Fig. 3. Temperature dependent magnetization of $Ba_{0.54}K_{0.46}Fe_2As_2$ single crystal under different magnetic field for (a) $H||c$ and (c) $H\perp c$ orientations. We have given offset to avoid overlapping. (b) Field dependence of the calculated critical current density from hysteresis loops using Bean critical state model at the temperatures just below the superconducting transition temperature for $H||c$ orientation to observe peak effect. Inset: shows three characteristic fields related to $J_c(H)$ curve. (d) The phase diagram of $Ba_{0.54}K_{0.46}Fe_2As_2$ single crystal. Solid lines are fitted curves using power law function.

recorded at different magnetic fields and we have given offset to avoid overlapping as shown in Fig. 3(c). We have taken the temperatures where bifurcation starts in the ZFC and FC curves. In Fig. 3(d) we have shown the vortex phase diagram of the material showing variation of different characteristic fields, e.g., H_{sp}, H_{min}, and magnetically determined upper critical field (H_{c2}^m). Here we have tried to fit the H_{min} and H_{sp} curves using $H_{min}(T) = H_{min}(0) \times (1 - T/T_c)^n$ and $H_{sp}(T) = H_{sp}(0) \times (1 - T/T_c)^n$. The solid lines are the fitted curves with $H_{min}(0) = 179\ kOe$ and $n = 1.1$. For $H_{sp}(T)$ we have obtained $H_{sp}(0) = 210\ kOe$ and $n = 0.8$. The same power law has been used previously by Yang et al. [26] to explain the vortex phase diagram of hole doped $Ba_{1-x}K_xFe_2As_2$ single crystal. For $H_{min}(T)$, Yang et al. have got $n = 1.3$ and $n = 1.5$ for H_{sp}. In some electron doped compound like $Ba(Fe_{1-x}Co_x)_2As_2$, Shen et al. [30] have also used power law fittings to study vortex phase diagram. They have obtained $n = 1.4$ for H_{sp} and $n = 1.2$ for H_{irr}. So our results are very similar to the previously reported results. The similar power law behavior in $H_{sp}(T)$ is found in YBCO [31] and oxygen free LiFeAs compound [32]. From the careful observation of the experimental data, it is seen that at a temperature of 36 K second peak occurs at a magnetic field of 27.49 kOe in $H||c$ orientation (shown in inset picture of Fig. 3(b)) and current density vanishes at 56.04 kOe. So in this compound, peak effect and vortex-glass melting occur at different regions of the vortex phase diagram. This is a characteristics feature in the case of glassy transition (exists in our compound as shown below) where there are large number of weak point defects in the material. Below the peak of J_c, pinned vortices creep due to thermal fluctuation and above the peak plastic flow occurs. J_c completely goes to zero at H_{irr}, which implies that after H_{irr} vortex exists without any pinning.

3.2. Flux dynamics and nature of vortex melting transition using ac susceptibility

In this section we have investigated the evolution of irreversibility temperature under different field and frequency conditions and the microscopic nature of transition using ac susceptibility technique. In ac magnetic measurements, the magnetization periodically changes in response to the applied ac field. High temperature superconductors (HTS) often exhibit nonlinear magnetic behavior in application of ac field due to nonlinear flux diffusion in the vortex region. So the application of a pure sinusoidal field $B(t) = B_{ac}\cos(2\pi ft)$ induces a non-sinusoidal oscillation of the magnetization M(t). This oscillation can be expressed as a sum of sinusoidal components with harmonics of the driving frequency.

$$\mu_0 M(t) = B_{ac} \sum_{n=1}^{\infty} \left[\chi_n' \cos(2\pi nft) + \chi_n'' \sin(2\pi nft) \right] \tag{1}$$

where $\chi_n' = \frac{\mu_0}{\pi B_{ac}} \int_0^{2\pi} [M(t)\cos(2\pi nft)]d(2\pi ft)$, $\chi_n'' = \frac{\mu_0}{\pi B_{ac}} \int_0^{2\pi} [M(t)\sin(2\pi nft)]d(2\pi ft)$ are in phase and out of phase components of harmonics, respectively and n is an integer. We can express it in the complex notation by $\chi_n = \chi_n' - i\chi_n''$. If the response is linear then we will get only first or fundamental harmonics corresponding to $n = 1$ and higher harmonics, e.g., second ($n = 2$), third ($n = 3$) if the response is nonlinear. Here we have presented fundamental as well as ac higher harmonic susceptibility studies for determination of flux dynamics and order of vortex-melting transition in single crystal BaK122 superconductors. Fig. 4(a) shows the temperature dependence of real part (χ') of the fundamental ac-susceptibility at
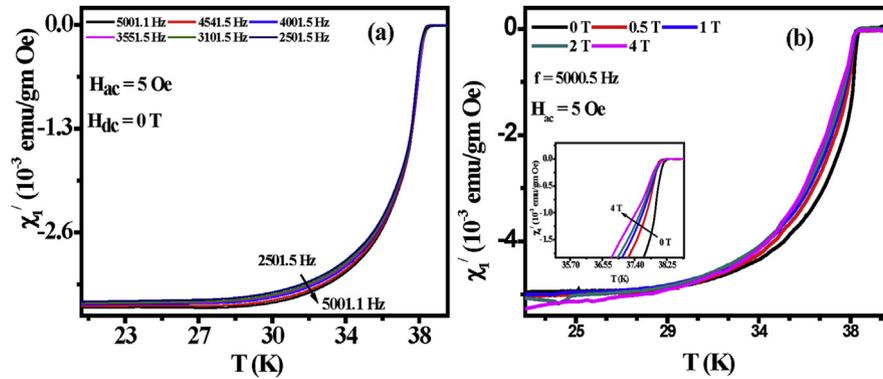
Fig. 4. (a) Temperature variation of χ' for several frequencies of Ba$_{0.54}$K$_{0.46}$Fe$_2$As$_2$ single crystal measured for $H_{ac} = 5$ Oe and $H_{dc} = 0$ Oe. (b) Temperature variation of χ' for several dc magnetic fields of Ba$_{0.54}$K$_{0.46}$Fe$_2$As$_2$ single crystal measured for $H_{ac} = 5$ Oe and $f = 5000.5$ Hz. Both ac and dc magnetic fields applied perpendicular to the c-axis. Inset: shift of diamagnetic onset with magnetic field in an extended scale.

several frequencies with ac magnetic field amplitude $h_{ac} = 5$ Oe and $h_{dc} = 0$ Oe. The experimental results show that the frequency of the ac magnetic field does not affect the fundamental harmonic susceptibility versus temperature curves strongly. Real part (χ'_1) versus temperature (T) curve has identical shape for different frequency and χ'_1 increases with frequency clearly indicating the presence of a certain time scale for vortex motion. The frequency dependence of fundamental susceptibility is not explained by critical state model since it assumes that the magnetic response of the material is independent of the frequency of the applied alternating field. In the temperature region which is far below from T_c, χ'_1 strongly depends on frequency, in contrast with the prediction of critical state model. However, this discrepancy shrinks in the region close to T_c. The data close to T_c is well described by the critical state model. Fig. 4(b) shows temperature dependence of χ'_1 at several dc magnetic fields up to 40 kOe with applying 5 Oe ac magnetic field at a particular frequency. Here both magnetic fields have been applied along perpendicular to the c-axis. The main feature of the $\chi'_1(T)$ curves is the shift of diamagnetic onset towards the lower temperature with increasing dc magnetic field as shown in inset of Fig. 4(b). In the present paper we concentrate on the frequency dependence of the irreversibility temperature (T_{irr}) which we can determine from the onset of third harmonic signal. The basic idea behind this is that the existence of irreversibility will produce harmonics. The temperature dependence of the third harmonic susceptibility (χ_3) has been measured at a frequency of 5000.5 Hz with different dc field up to

70 kOe. Fig. 5(a) shows the temperature variation of χ_3 with different dc fields keeping ac field fixed at 5 Oe and frequency 5000.5 Hz. We have observed from the figure that χ_3 rises abruptly when sample is cooled from above T_c and decreases slowly after crossing the peak. The onset of χ_3 is weakly dc field dependent and it reflects a sharp transition (T_{irr}) from a reversible to an irreversible state when moving from above T_c. The decreasing part of χ_3 and peak is strongly affected by the dc magnetic field as shown in the figure. Inset of Fig. 5(a) shows the variation of irreversibility temperature with magnetic field which separates reversible vortex liquid (VL) and irreversible vortex glass (VG) phases. This line is actually called irreversibility line (IL). The points are taken from the onset of third harmonic signal with different magnetic fields from Fig. 5(a). Fig. 5(b) shows the temperature variation of χ_3 with different ac fields keeping frequency at 5000.5 Hz. Here we have observed that with increasing ac field, χ_3 peak height decreases and T_{irr} strongly depends on ac field (shown in inset of Fig. 5(b)). Now we are going to discuss how the T_{irr} and T_{peak} depend on frequency when dc and ac fields are kept fixed. With increasing frequency, penetration depth of the ac field decreases which results the decrease of peak height with increasing frequency. Fig. 6(a) shows the temperature variation of real part of the third harmonic susceptibility (χ'_1) with different frequencies keeping ac field fixed at 5 Oe. Here main point is that T_{irr} strongly depends on frequency and this dependency increases with dc magnetic field. It is clearly shown in the Fig. 6(b) and (c). Fig. 6(d) shows the temperature
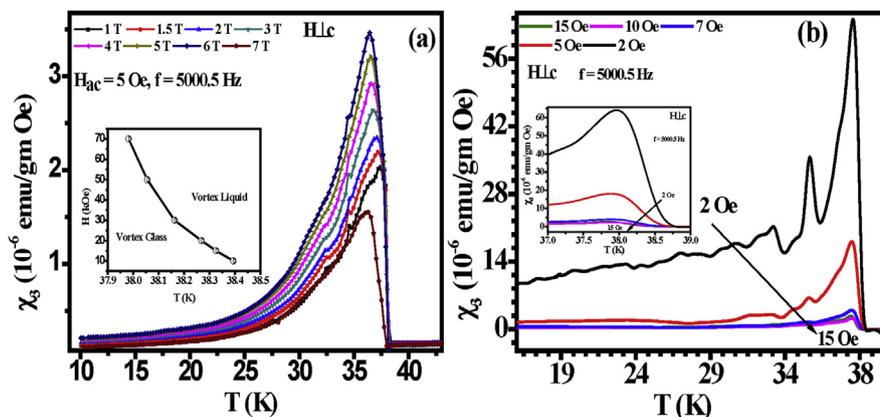
Fig. 5. (a) Temperature variation of the amplitude of the third harmonic susceptibility of Ba$_{0.54}$K$_{0.46}$Fe$_2$As$_2$ single crystal for several dc magnetic fields measured for $H_{ac} = 5$ Oe and $f = 5000.5$ Hz. Inset: irreversibility line obtained from the shift of third harmonic onset with magnetic field. (b) Temperature variation of the amplitude of the third harmonic susceptibility for several ac magnetic fields measured for $f = 5000.5$ Hz. Inset: shift of third harmonic onset with ac magnetic field in an extended scale.
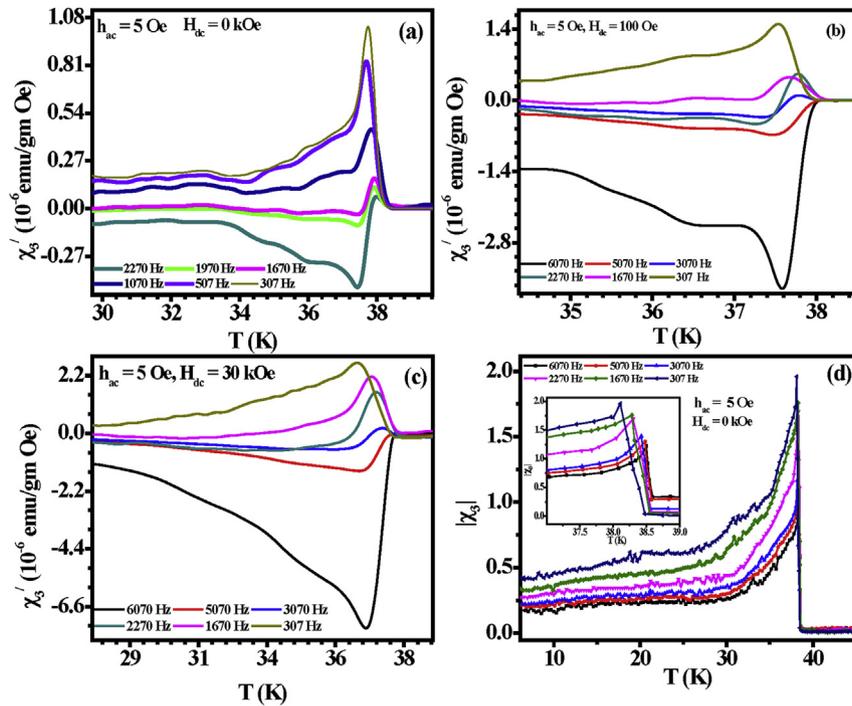
Fig. 6. Temperature variation of real part of the third harmonic susceptibility for several frequencies of Ba$_{0.54}$K$_{0.46}$Fe$_2$As$_2$ single crystal measured for H_{ac} = 5 Oe and (a) H_{dc} = 0 Oe (b) H_{dc} = 100 Oe (c) H_{dc} = 30 kOe. (d) Temperature variation of magnitude of the third harmonic susceptibility($|\chi_3|$) with different frequencies keeping ac field fixed at 5 Oe and without dc field. Inset shows the variation of χ_3 with temperature in an extended scale clearly showing the increase of T_{irr} with increasing frequency.

variation of magnitude of the third harmonic susceptibility($|\chi_3|$) with different frequencies keeping ac field fixed at 5 Oe and without applying any dc field. Inset of Fig. 6(d) shows the variation of χ_3 with temperature in an extended scale clearly showing the increase of T_{irr} with increasing frequency. From the Fig. 6(d) we have seen that the peak temperature (T_{peak}) moves to the higher temperature side with increasing frequency, exactly opposite to the increasing magnetic field as discussed in the above. Fig. 7 shows the temperature variation of imaginary part of the third harmonic susceptibility (χ_3'') with different frequencies keeping ac field fixed at 5 Oe and dc field 0 kOe (Fig. 7(a)) and 30 kOe (Fig. 7(b)). These also represent the same behavior as for the real part and only difference is that peak resides in opposite side. The variation of peak height and peak temperature with applied dc magnetic field is shown in the Fig. 8(a). From the figure we see that peak temperature (T_{peak}) continuously moves to the lower temperature with

increasing dc field. The peak is obtained when the alternating field fully penetrates the sample and when dc field increases it occurs at lower temperature. But for the case of peak height, trend is little bit different. With increasing magnetic field up to 60 kOe peak height increases gradually and then suddenly a small peak (reduced peak height) is obtained at 70 kOe magnetic field. It is well known that third harmonic susceptibility χ_3 is a measure of nonlinear dissipation only whereas out of phase susceptibility (χ_1'') is a measure of linear and nonlinear dissipation. In presence of high magnetic field, the total field is almost constant which removes the observation of field dependence of flux flow and thermally activated flux flow (TAFF) and generates a linear diffusion process of the magnetic field. So in the high magnetic field nonlinear process is suppressed, which results the decrease in third harmonic signal at very high magnetic field. In Fig. 8(b) we have shown the frequency variation of onset temperature $T(|\chi_3|_{onset})$ of third harmonic signal for
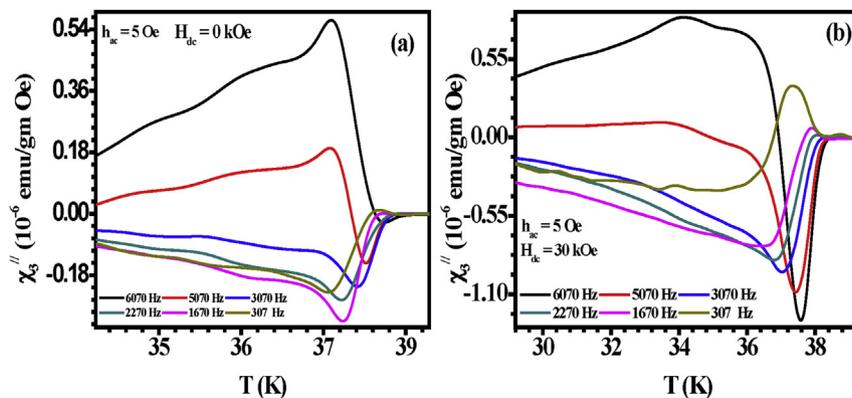
Fig. 7. Temperature variation of imaginary part of the third harmonic susceptibility for several frequencies of Ba$_{0.54}$K$_{0.46}$Fe$_2$As$_2$ single crystal measured for H_{ac} = 5 Oe and (a) H_{dc} = 0 Oe (b) H_{dc} = 100 Oe.
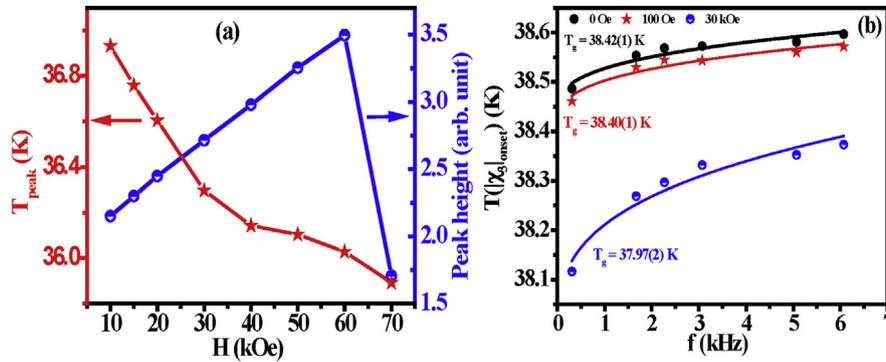
Fig. 8. (a) The variation of peak temperature and peak height with applied dc magnetic field, (b) Frequency dependence of the irreversibility point T($|\chi_3|_{onset}$) for three different dc magnetic fields, e.g., 0 Oe, 100 Oe and 30 kOe, all measured from the onset of third harmonic signal. The solid lines are fitting curves to Eq. (2).

several dc fields. From the figure it is clear that onset temperatures increase with frequency (also shown in Fig. 6(d) for zero dc field). This onset temperature is a significant point which separates VG from VL states. To explain the frequency dependence of the irreversible temperature there are two models: thermally-activated flux motion (TAFM) approach and vortex-glass phase transition model. In the scenario of TAFM, gradual freezing of fluxons in their pinning centers determines the magnetic irreversibility and above the irreversibility temperature depinning of fluxons occurs due to thermal activation within the time scale of the experiment which leads to $T_{irr} = 0$ for time scales approaching infinity. On the other hand in the vortex-glass phase transition model transition temperature (T_g) is the irreversible temperature when time scale approaches infinity, i.e., $f \rightarrow 0$. For a second-order phase transition, universal critical scaling behavior near the vortex-glass phase transition temperature (T_g) is expected. Near T_g critical slowing of the dynamics is expected with a power-law divergence of the relaxation time [1,33]. Here we have interpreted our experimental frequency dependence of the irreversible temperature in the framework of vortex-glass phase transition model. For a second-order phase transition at T_g, power-law divergence of the correlation length $\xi \propto |T - T_g|^{-\nu}$ is expected, where ν is a critical exponent [1,33]. Critical slowing down of the dynamics is also expected near T_g with relaxation time $\tau \propto |T - T_g|^{-\nu z}$, where z is a dynamical critical exponent. From the above relationship one can write the frequency dependence of the irreversible temperature for a D dimensional system [1,33]:

$$T_{irr}(H,f) = T_g(H) + A(H)f^{1/\nu(z+2-D)} \qquad (2)$$

where $T_{irr}(H,0)$ is identified with $T_g(H)$ and A(H) is a coefficient depending on the applied magnetic field. The solid lines in Fig. 8(b) represent the fitted curves to the experimental data using Eq. (2) for dc magnetic fields of 0 Oe, 100 Oe and 30 kOe. We have calculated the parameters ν and z following the same procedure used by Kim et al. [34] We have obtained z = 4.2 and ν = 1, which are in good agreement with the values ($\nu \sim 1-2$ and z > 4) predicted by Vortex Glass (VG) theory [1,33]. We have used D = 3 since there are some reports which explain three dimensional nature [35] of $Ba_{1-x}K_x Fe_2As_2$ with no predicted dimensionality crossover induced by fields. We have fitted (shown in Fig. 8(b)) frequency dependent T_{irr} data using Eq. (2) and obtained T_g values are 38.42(1) K, 38.40(1) K and 37.97(2) K for dc magnetic fields of 0 Oe, 100 Oe and 30 kOe, respectively. So our experimental observation clearly indicates that frequency variation of T_{irr} is well explained by the framework of vortex-glass phase transition model and the order of vortex-glass phase transition is second-order in nature. This conclusion is also

supported by recent specific-heat and thermal expansion measurements of $Ba_{0.5}K_{0.5}Fe_2As_2$ single crystal [16]. Another important thing is that the moderate fluctuation in Fe-based superconductors relative to cuprates has also some effect on the vortex-glass transition. To explain this effect more clearly, one needs more theoretical understanding of the vortex-glass transition in a magnetic field within the fluctuation region. To understand different frequency variation of T_{irr} among various Fe-based superconductors more experimental works are required on high quality single crystals.

4. Summary

In summary, we report the experimental observation of second order vortex-glass melting transition in an optimally doped p-type iron-based superconductor $Ba_{0.54}K_{0.46}Fe_2As_2$ through ac susceptibility measurements under various fields and frequency conditions. Magnetic irreversible temperature (T_{irr}) of a superconductor is a significant transition temperature from a state of dissipative flux motion without pinning to a state of flux pinning and has a great importance from technological point of view. From the dc magnetization measurements, we have observed that peak effect (PE) and vortex glass melting transition occur at different regions in the vortex phase diagram and it is a characteristic feature of a glassy transition. From fundamental and higher harmonic susceptibility measurements, we have observed that T_{irr} strongly depends on frequency in this compound. This frequency dependence can be explained in the framework of vortex-glass phase transition model. All the experimental results suggest that vortex-glass melting transition is a second order in nature. One can conclude that thermal fluctuations and level of defects control the overall vortex dynamics in this compound. Nevertheless, more experimental and theoretical studies are necessary in order to understand clearly the overall vortex dynamics in this compound as well as other iron-based superconductors.

References

[1] M.P.A. Fisher, Phys. Rev. Lett. 62 (1989) 1415.
[2] S. John, T. Lubensky, Phys. Rev. B 34 (1986) 4815.
[3] Z.-A. Ren, W. Lu, J. Yang, Y.Q. Wu, X.-L. Shen, Z.-C. Li, G.-C. Che, X.-L. Dong, L.-L. Sun, F. Zhou, Chin. Phys. Lett. 25 (2008) 2215.
[4] Y. Kamihara, T. Watanabe, M. Hirano, H. Hosono, J. Am. Chem. Soc. 130 (2008) 3296.
[5] G.F. Chen, Z. Li, G. Li, J. Zhou, D. Wu, J. Dong, W.Z. Hu, P. Zheng, Z.J. Chem, H.Q. Yuan, J.L. Luo, N.L. Wang, Phys. Rev. Lett. 101 (2008) 057007.
[6] H. Chen, Y. Ren, Y. Qiu, W. Bao, R.H. Liu, G. Wu, T. Wu, Y.L. Xie, X.F. Wang, Q. Huang, X.H. Chen, Europhys. Lett. 85 (2009) 17006.
[7] V.J. Emery, S.A. Kivelson, Nat. Lond. 374 (1995) 434.
[8] C. Meingast, V. Pasler, P. Nagel, A. Rykov, S. Tajima, P. Olsson, Phys. Rev. Lett. 86 (2001) 1606.
[9] S.W. Pierson, T.M. Katona, Z. Tesanovic, O.T. Valls, Phys. Rev. B 53 (1996) 8638.
[10] Z. Tesanovic, Phys. Rev. B 59 (1999) 6449.
[11] N. Overend, M.A. Howson, I.D. Lawrie, Phys. Rev. Lett. 72 (1994) 3238.
[12] R. Lortz, C. Meingast, A.I. Rykov, S. Tajima, Phys. Rev. Lett. 91 (2003) 207001.
[13] G. Blatter, M.V. Feigelman, V.B. Geshkenbein, A.I. Larkin, V.M. Vinokur, Rev. Mod. Phys. 66 (1994) 1125.
[14] U. Welp, C. Chaparro, A.E. Koshelev, W.K. Kwork, A. Rydh, N.D. Zhigadlo, J. Karpinski, S. Weyeneth, Phys. Rev. B 83 (2011), 100513(R).
[15] C. Chaparro, L. Fang, H. Claus, A. Rydh, G.W. Crabtree, V. Stanev, W.K. Kwok, U. Welp, Phys. Rev. B 85 (2012) 184525.
[16] H.K. Mak, P. Burger, L. Cevey, T. Wolf, C. Meingast, R. Lortz, Phys. Rev. B 87 (2013) 214523.
[17] Y. Wolfus, Y. Abulafia, L. Klein, V.A. Larkin, A. Shaulov, Y. Yeshurun, M. Konczykowski, M. Feigel'man, Phys. C 224 (1994) 213—220.
[18] C.P. Bean, Rev. Mod. Phys. 36 (1964) 31.
[19] E.M. Gyorgy, R.B. van Dover, K.A. Jackson, L.F. Schneemeyer, J.V. Waszczak, Appl. Phys. Lett. 55 (1989) 283.
[20] C. Zhang, M. Wang, H. Luo, M. Wang, M. Liu, J. Zhao, D.L. Abernathy, T.A. Maier, K. Marty, M.D. Lumsden, S. Chi, S. Chang, J.A. Rodriguez-Rivera, J.W. Lynn, T. Xiang, J. Hu, P. Dai, Sci. Rep. 1 (2011) 115.
[21] G. Mu, H. Luo, Z. Wang, L. Shan, C. Ren, H.-H. Wen, Phys. Rev. B 79 (2009) 174501.
[22] M. Rotter, M. Tegel, D. Johrendt, Phys. Rev. Lett. 101 (2008) 107006.
[23] R. Lortz, N. Musolino, Y. Wang, A. Junod, N. Toyota, Phys. Rev. B 75 (2007) 094503.
[24] M. Pissas, S. Lee, A. Yamamoto, S. Tajima, Phys. Rev. Lett. 89 (2002) 097002.
[25] For Bi-based cuprates Y. Yeshurum, N. Bontemps, L. Burlachkov, A. Kapitulnik, Phys. Rev. B 49 (1994), 1548(R); G. Yang, P. Shang, S.F. Sutton, I.P. Jones, J.A. Abell, C.E. Gough, ibid. 48 (1993) 4054. For Tl-based cuprates, V. Hardy, A. Wahl, A. Ruyter, A. Maignan, C. Martin, L. Coudrier, J. Provost, Ch. Simon, Physica C 232, (1994) 347.
[26] H. Yang, H. Luo, Z. Wang, H.-H. Wen, Appl. Phys. Lett. 93 (2008) 142506.
[27] W. Zhou, X. Xing, W. Wu, H. Zhao, Z. Shi, Sci. Rep. 6 (2016) 22278.
[28] M.A. Tanatar, N. Ni, C. Martin, R.T. Gordon, H. Kim, V.G. Kogan, G.D. Samolyuk, S.L. Bud'ko, P.C. Canfield, R. Prozorov, Phys. Rev. B 79 (2009) 094507.
[29] W. Zhou, J. Zhuang, F. Yuan, X. Li, X. Xing, Y. Sun, Z. Shi, Appl. Phys. Exp. 7 (2014) 063102.
[30] B. Shen, P. Cheng, Z. Wang, L. Fang, C. Ren, L. Shan, H.-H. Wen, Phys. Rev. B 81 (2010) 014503.
[31] L. Klein, E.R. Yacoby, Y. Yeshurun, A. Erb, G. Muller-Vogt, V. Breit, H. Wuhl, Phys. Rev. B 49 (1994), 4403(R).
[32] A.K. Pramanik, L. Harnagea, C. Nacke, A.U.B. Wolter, S. Wurmehl, V. Kataev, B. Buchner, Phys. Rev. B 83 (2011) 094502.
[33] D.S. Fisher, M.P.A. Fisher, D.A. Huse, Phys. Rev. B 43 (1991) 130.
[34] H.—J. Kim, Y. Liu, Y.S. Oh, S. Khim, I. Kim, G.R. Stewart, K.H. Kim, Phys. Rev. B 79 (2009) 014514.
[35] S. S.- Sugui Jr., L. Ghivelder, A.D. Alvarenga, J.L. Pimentel Jr., H. Luo, Z. Wang, H.-H. Wen, Phys. Rev. B 80 (2009) 014518.